Spectral and Microscopic Investigation of Betamethasone/ Cyclodextrin Covered Ag/Co/ Nanorods

Ayyadurai Mani[1], Narayanasamy Rajendiran[1*], Poomalai Senthilraja[2], S. Senthilmurugan[3]

[1] Department of Chemistry, Annamalai University, Annamalai Nagar, Tamilnadu, India

[2] Department of Bioinformatics, Bharathidasan University, Tiruchy, Tamilnadu, India

[3] Department of Zoology, Annamalai University, Annamalai Nagar, Tamilnadu, India

***Corresponding Author**

DOI: https://dx.doi.org/10.51244/IJRSI.2026.1303000237

Received: 27 March 2026; 02 April 2026; Published: 21 April 2026

ABSTRACT

Silver/cobalt/betamethasone/cyclodextrin nanoparticles are synthesized and characterized by UV-visible, fluorescence, FE-SEM, TEM, differential scanning colorimeter, FTIR, and XRD methods. Single emission was observed in α-CD and β-CD. Compared to the BEM/CD inclusion complex, a red or blue shifted absorption and fluorescence maximum was seen in Ag/BEM/β-CD and Ag/Co/BEM/β-CD nanoparticles. Nanoparticle size was measured by TEM-EDS and XRD methods. TEM images showed nanorods are formed in Ag/BEM/β-CD and Ag/Co/BEM/β-CD. Antibacterial activity results revealed that the Ag/BEM/β-CD and Ag/Co/BEM/β-CD nanomaterials show more antibacterial activity than isolated BEM drug. Further, BEM exhibits anticancer activity against the 2oh4 protein.

Keywords: Betamethasone, Cyclodextrin, Inclusion complex, Silver nano, Nanorod,

INTRODUCTION

Silver nanoparticles with exclusive optical, electronic, and antibacterial properties have been commonly used in biosensing, photonics, electronics, antimicrobial applications, etc., among others [1-6]. Ag nanoparticles have strong antimicrobial activity, which induced major direction for the development of Ag nanoparticle products, including textiles, food storage containers, antiseptic sprays, catheters, and bondages. The biocidal action of silver nanoparticles depends on their size, shape, and surface coatings. Cobalt and cobalt oxide nanoparticles have various biomedical applications because of their distinctive antioxidant, antimicrobial, antifungal, anticancer, larvicidal, antileishmanial, anticholinergic, wound-healing, and antidiabetic properties [7, 8].

Hence, the synthesis of silver nanoparticles with different methods for physiological application in humans is necessary to expand their biomedical applications. Because of the variety of uses for silver and cobalt nanoparticles, it is essential to discover a new approach for this nanoparticle's synthesis. For the synthesis of silver nanoparticles, a number of physical and chemical approaches have been published [9-21], however the spectral characteristics of the silver with cobalt nano and drug-cyclodextrin inclusion complex method have not yet been reported. In this regard, we synthesise silver with cobalt and drug-cyclodextrin nanoparticles. The aim of the work is, a) to analyse the effect of silver and silver/cobalt nanoparticles on the betamethasone-cyclodextrin (BEM:CD) inclusion complex, b) to find which type of nanomaterials is formed, and c) to analyse the antibacterial and anticancer activity of the drug and the nanomaterials.

Bromhexine (Fig.1) is chemically known as benzene methenamine, 2,4-dibromo-6-((cyclohexyl(methyl)amino)methyl) aniline, or alternatively, N-cyclohexyl-N-methyl-(2-amino-3,5-dibromobenzyl)amine. It is commonly used to reduce mucus viscosity and facilitate its clearance in conditions associated with excessive mucus production such as the common cold, influenza, respiratory tract infections,

ISSN No. 2321-2705 | DOI: 10.51244/IJRSI |Volume XIII Issue III March 2026

and other related ailments. These disorders typically involve airway inflammation, increased mucus secretion, and impaired mucociliary clearance. In cases of suspected or mild COVID-19, bromhexine is being studied as a mucolytic agent to help alleviate chest discomfort and coughing. Interestingly, it also acts as a selective inhibitor of the transmembrane serine protease 2 (TMPRSS2), which plays a role in viral entry into host cells. This function gives bromhexine potential antiviral properties due to its strong inhibition of TMPRSS2.

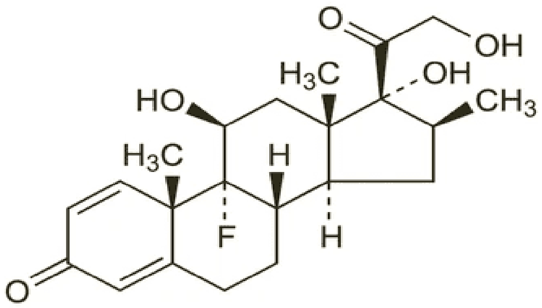

Figure 1. Chemical structure of betamethasone (BEM).

Experimental

Preparation of Drug/CD inclusion complex in solution

Different concentrations (0.1 to 1.0×10-2 M) of α-CD or β-CD solution were taken in a 10-milliliter standard measuring flask. The concentration of the BEM stock solution is 2×10-2 M. The BEM stock solution (0.1 or 0.2 ml) was added to the aforementioned flasks. After vigorously stirring the mixture, 10 milliliters of triple-distilled water were added to dilute it. Each flask's final drug concentration was 4×10-4 M. The trials were conducted at a temperature of 298 K.

Preparation of silver and silver/cobalt nanoparticles

In 200 ml of deionized water, 0.01 M of silver nitrate was dissolved, and the solution was heated to between 50 and 60 °C for 20 to 30 minutes. With vigorous stirring, one to two ml of 1% trisodium citrate (1 g dissolved in 100 ml deionized water) was added to this solution. Ag nanoparticle production is confirmed by the appearance of a pale-yellow color [22-25].

In the above warmed silver nanoparticle solution (100 ml), 0.01 M cobalt sulphate dissolved in deionized water (50 ml) was gradually added with constant stirring. 100 ml of the Ag nano solution and 150 ml of the Ag/Co nano solution were frozen and dried (mini-lyophilized) at -80 °C. The powder samples of Ag and Ag/Co were collected and used for additional analysis.

Preparation of Ag /BEM/CD inclusion complex nanomaterials

BEM drug (2×10^{-3} M) dissolved in 20 ml of ethanol was added gradually to the CD (1×10^{-2} M in 80 ml) in deionized water. Using a hot plate with a magnetic stirrer, this mixture was heated to 50 °C for two hours. Then the silver nano solution (0.01 M in 50 ml) was added to the above BEM/CD inclusion complex solution (50 ml) and mixed for one to two hours.

The same method was used to make nanomaterial made of Ag/Co/BEM/CD. 50 ml of the Ag/Co nanoparticle solution was added to the BEM/CD inclusion complex (50 ml). After that, the above two solutions were frozen and dried (mini-lyophilized) at -80 °C. The powder samples of Ag/BEM/CD and Ag/Co/BEM/CD were collected and used for further analysis.

Molecular Modeling Studies

The Molecular geometry of BEM, CD, and its inclusion complexes was analyzed using Spartan 08, a molecular modeling program. The semi-empirical PM3 method in the gas phase and Gaussian 09W software

ISSN No. 2321-2705 | DOI: 10.51244/IJRSI |Volume XIII Issue III March 2026

were used to theoretically determine the most stable complexation energy following the structural assembly of two orientation inclusion complexes.

Antibacterial Activity

It is designed to test the ability of the newly synthesized materials that have been treated with antibacterial agents to prevent antibacterial growth and to kill microorganisms. By using the disc diffusion method, the antibacterial activity of BEM was evaluated against bacterial pathogens. ISO 20743 is a 'quantitative test' used to determine the antibacterial activity of all antibacterial products. For the disc diffusion assay, neomycin (30 µg/disc) and nystatin (100 IU/disc) were used as positive controls for antibacterial and antifungal activities, respectively. On the Muller Hinton agar plates, every bacterial strain was dispersed separately.

Ciprofloxacin was used as the standard antibiotic. A volume of 100 µl of test compound and 100 µl of cells were added to wells on a 96-well plate, making a total of 200 µl in each well. This was followed by 24 hours incubation. After 24 hours of incubation, the MTT assay was carried out to determine the cell viability.

The standard plate count method consists of diluting a sample with sterile saline or phosphate buffer diluent until the bacteria are dilute enough to count accurately. That is, the final plates in the series should have between 30 and 300 colonies.

The sensitivity status of the bacteria is determined by measuring the inhibition zone diameter to the nearest whole millimeter, which defines the bacteria as resistant (≤ 9 mm), moderately sensitive (10-11 mm), or sensitive (≥12 mm) to the antibiotic.

In order to do this, a bacterial pathogen was inoculated in nutrient broth and cultured for 1–2 hours before an antibacterial experiment. The disc was loaded with various quantities (25 l, 50 l, 75 l, 100 l) of olanzapine or Ag/BEM/CD or Ag/Co/BEM/CD and then incubated for 24 hours at 37 °C. The assay was performed three times. After the incubation time was over, the zone of inhibition was measured in millimeters.

AutoDocking Method

AutoDock is a widely used software suite for automated molecular docking. It incorporates algorithms such as simulated annealing, local gradient search, and genetic algorithms [26–31]. AutoDock 4.2.6 and AutoDock Vina were used in this study. Docking was performed using the Lamarckian Genetic Algorithm (LGA) combined with the Solis & Wets local search method. Initial positions, orientations, and torsional angles of ligands were randomly assigned. Each docking run consisted of 10 independent simulations with a maximum of 2.5×10^5 energy evaluations per run. The population size was set to 150, with translational step sizes of 0.2 Å and rotational/torsional step sizes of 5°.

RESULT AND DISCUSSION

UV-Visible and emission spectral studies

Absorption and emission spectral maxima of the betamethasone (BEM, Fig.1) drug were measured with and without α-CD and β-CD and the corresponding information is given in Table 1, and Fig.2. In water, α-CD and β-CD, the absorption maxima of BEM were appearing at 243, 220 nm. No notable changes were noticed in the maxima, however, the absorbance slightly raised as the concentrations of α-CD and β-CD were increased in the BEM solution. At 367 nm, BEM exhibits single emission maximum in water, α-CD and β-CD (Fig. 2). As α-CD and β-CD concentrations rose, the emission intensity was increased at the same wavelength indicating that the BEM molecule was entrapped into the CD cavities. The CD cavity provides a non-polar environment and restricts the free rotation of the guest molecules; hence, the absorption and emission intensities of the BEM molecule were slightly raised [32–40].

Table 1. Absorption and fluorescence spectral maxima of BEM with different α-CD and β-CD concentrations

Concentration of CD $x10^{-3}$M	**α-CD**			**β-CD**		
	λ_{abs}	**log ε**	**λ_{flu}**	**λ_{abs}**	**log ε**	**λ_{flu}**
BEM only (Without CD)	243 220	3.86 4.31	367	243 220	3.86 4.31	367
0.1	243 220	3.87 4.32	368	244 221	3.89 4.32	368
0.2	243 220	3.88 4.32	368	244 221	3.91 4.32	368
0.4	243 220	3.89 4.33	368	244 221	3.92 4.33	368
0.6	243 220	3.90 4.33	368	244 221	3.93 4.33	368
0.8	243 220	3.91 4.33	368	244 221	3.94 4.34	368
1.0	243 220	3.93 4.34	368	244 221	3.95 4.34	368
Excitation wavelength (nm)	-	-	250	-	-	250
K (1:1) $x10^5$ M^{-1}	138	-	53	175	-	143
ΔG ($kcalmol^{-1}$)	-12.4	-	-10.0	-13.0	-	-12.5

From the slope and intercept of the Benesi-Hildebrand plot, the binding constant and stoichiometry ratio of the BEM/CD for the inclusion complexes was estimated. The presence of an isosbestic point and the formation of the 1:1 inclusion complex is indicated by the plot of $1/(A-A_0)$ versus 1/[CD] and $1/(I-I_0)$ vs. 1/[CD] [32–40]. The negative free energy change (ΔG) values (Table 1), reveal that the binding process was spontaneous and thermodynamically stable at the experimental temperature.

To know the inclusion complexation process, the absorption and emission spectra of the BEM molecule were examined in different solvent polarities. Absorption and emission maxima of the BEM molecule are red shifted from non-polar to polar solvents. In all the solvents, BEM molecules exhibit a single emission. The red or blue shift in the absorption and emission spectral maximum reflects increased delocalization of the C=O group and π-cloud of the conjugated double bonds [41,42]. The absorption and emission spectral shifts are different in the solvents and the CD solution suggests a BEM molecule encapsulated in the CD cavity.

ISSN No. 2321-2705 | DOI: 10.51244/IJRSI |Volume XIII Issue III March 2026

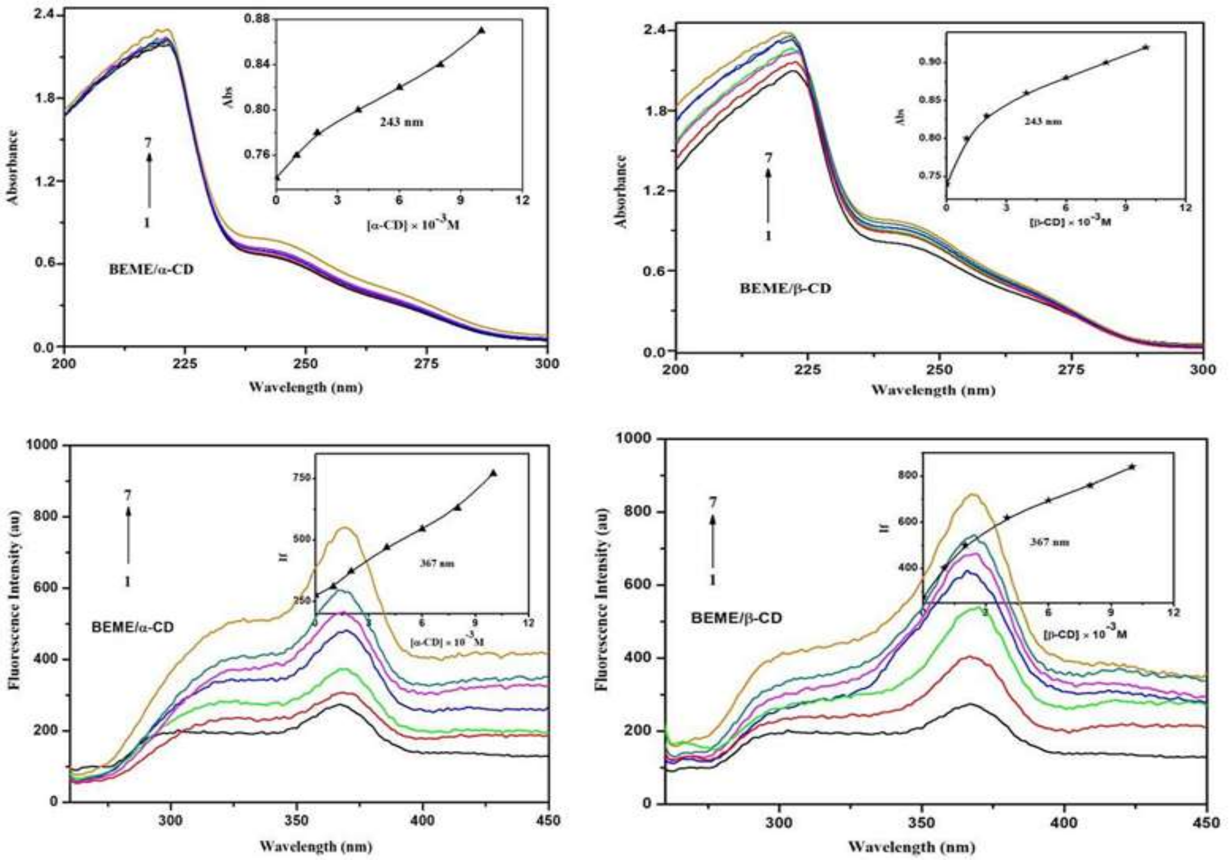

Figure 2. Absorption and fluorescence spectra of BEM in different α-CD and β-CD concentrations (M): (1) 0, (2) 0.001, (3) 0.002, (4) 0.004, (5) 0.006, (6) 0.008, (7) 0.01. Insert figure: Absorbance and Fluorescence intensity *vs* [α-CD] and [β-CD].

Molecular Modeling

The ground state geometries of BEM, α-CD, β-CD, and their inclusion complexes were optimized using the semi-empirical PM3 approach. Table 2 lists the HOMO and LUMO (Fig. 3) and various thermodynamic parameter values of the BEM, α-CD, β-CD and the inclusion complex. The above- mentioned values for the BEM, α-CD and β-CD are significantly different in the inclusion complex because the polarity of the CD changed after the BEM entered into the CD cavity. The red and sky-blue colors indicate oxygen and fluorine atoms, respectively, while green and red colors in HOMO-LUMO denote negative and positive phases of the molecules. The red color in the molecular electrostatic potential (MEP) figure (Fig.3) shows that the electronegative charge of the atoms is greater than that of other atoms.

The BEM and CDs may generate one of two distinct inclusion complexes: (i) C=O substituted ring may encapsulate, or (ii) the $COCH_2OH$ group attached to the cyclic pentane ring may encapsulate in the CD cavity. In BEM, the horizontal bond distance is 11.05 Å and the vertical bond distance is 4.50 Å (Fig.3). The internal diameter of the α-CD and β-CD is approximately 5.6 and 6.5 Å and the height is 7.8 Å respectively. The vertical bond length of the BEM is shorter than the α-CD and □-CD cavity, hence the BEM drug is only partially encapsulated in the CD cavity.

Table 2. Energetic features, thermodynamic parameters and HOMO-LUMO energy calculations for BEM and its inclusion complexes by semiempirical PM3 method

Properties	**BEM**	**α-CD**	**β-CD**	**BEM/α-CD**	**BEM/β-CD**
E_{HOMO} (eV)	-10.37	-10.37	-10.35	-10.29	-10.37
E_{LUMO} (eV)	-0.73	1.26	1.23	-0.62	-1.11

ISSN No. 2321-2705 | DOI: 10.51244/IJRSI |Volume XIII Issue III March 2026

$E_{HOMO} - E_{LUMO}$ (eV)	9.64	-11.63	-11.58	9.67	9.25
Dipole (D)	3.74	11.34	12.29	11.96	12.98
E (kcal mol^{-1})	-236.00	-1247.62	-1457.63	-1487.64	-1702.88
ΔE (kcal mol^{-1})	-	-	-	-4.02	-9.25
G (kcal mol^{-1})	-319.39	-676.37	-789.52	998.08	-1023.75
ΔG (kcal mol^{-1})	-	-	-	-2.32	-85.16
H (kcal mol^{-1})	-270.32	-570.84	-667.55	-859.46	-1172.52
ΔH (kcal mol^{-1})	-	-	-	-18.3	-234.65
S (kcal/mol-Kelvin)	-0.164	-0.353	-0.409	-0.464	-0.489
ΔS (kcal/mol-Kelvin)	-	-	-	-0.053	-0.084
ZPE	303.07	635.09	740.56	940.19	1234.55

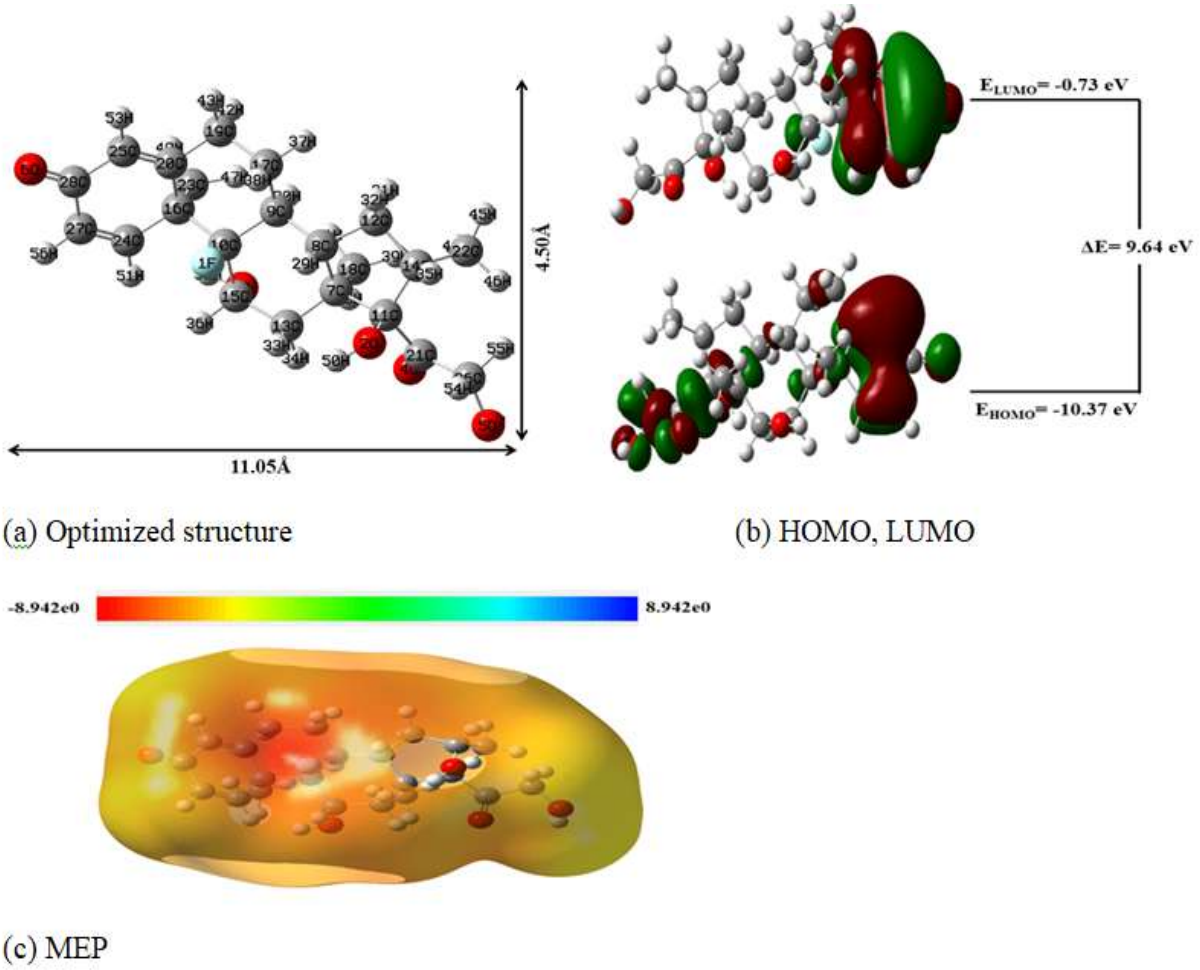

(a) Optimized structure

(b) HOMO, LUMO

(c) MEP

Figure 3. PM3 optimized structures of (a) BEM, (b) HOMO, LUMO and (c) MEP of BEM.

Absorption and emission spectral study of Ag and Ag/Co nanoparticles

In the solution phase, the absorption and emission spectra of the Ag, Ag/Co, Ag/BEM, Ag/β-CD, Ag/BEM/β-CD, Ag/Co/BEM, Ag/Co/β-CD and Ag/Co/BEM/β-CD nanoparticles are analyzed. The Ag nanoparticle's

ISSN No. 2321-2705 | DOI: 10.51244/IJRSI |Volume XIII Issue III March 2026

absorption and emission bond appears at 420, 250 nm and 350, 480 nm respectively. Further, the yellow color was identified for the Ag nanoparticles. When cobalt salt solution was added to the Ag nanoparticle solution, the above absorption and emission maxima changed to 405, 260 nm and 470, 366, 293 nm respectively. It is generally known that the particle size, shape, metallic material and surroundings all affect the plasmon resonance bonds of the absorption and emission and that the quantity of particles does not directly correlate with the intensity of the absorption and emission [43-45]. Due to surface plasmon resonance, it is known that Ag nanoparticles exhibit their highest absorption in the 400–500 nm range.

By adding the BEM solution to the Ag nano, the absorption maxima red shifted from 420, 250 nm to 438, 263 nm and the emission maxima red shifted from 480, 350 nm to 496, 358, 324 nm. Upon addition of β-CD solution to the Ag nanoparticles, the absorption maxima red shifted to 435, 257 nm and the emission maxima blue shifted to 472, 359, 323 nm. When the BEM/β-CD solution was added to the Ag nanoparticles, the absorption maxima were blue shifted to 407, 265 nm and the emission maxima shifted from 480, 350 nm to 445, 360, 296 nm, respectively.

While BEM molecules were added to the Ag/Co nano solution, the absorption maxima red shifted from 405, 260 nm to 460, 242 nm and emission maxima red shifted from 470, 366, 293 nm to 493, 483, 470, 360, 335 nm respectively. Upon addition of β-CD solution to the Ag/Co nanoparticles, the absorption maxima red shifted to 470, 277 nm and the emission maxima shifted to 469, 364, 337 nm respectively. Further, BEM: β-CD solution was added to the Ag/Co nanoparticles, the absorption maxima were shifted to 418, 256, 217 nm and the emission maxima shifted to 470, 361 nm respectively. The above red or blue shifts in the absorption and emission spectra suggest that Ag and Ag/Co nanoparticles were encapsulated in the CD cavity and interact with the BEM and CD molecules. Generally, if the guest is entrapped in the CD cavity, the intensity tends to increase or decrease, and the interaction is supported by spectral fluctuations.

FE-SEM and EDAX images

Ag nano, Ag/Co nano, BEM, Ag/BEM/β-CD and Ag/Co/BEM/β-CD nanomaterials were examined by FE-SEM and EDAX (Fig.4). The morphology images of the above materials demonstrate that all are different shapes. Ag has an oyster shape, Ag/Co has a marble rack or cloud shape, BEM drug has a marble rock shape, Ag/BEM/CD has a coastal stone shape and Ag/Co/BEM/CD also has a micro stone shape.

In accordance with FE-SEM-EDAX data, (a) Ag nano contains 58.31% silver nano and 41.69% oxygen, (b) Ag/Co nano solution comprises 44.08% silver, 38.47% cobalt and 17.45% oxygen, (c) BEM drug contains 72.12% carbon, 25.03% oxygen and 2.85% fluorine, (d) The composition of Ag/BEM/β-CD is 42.68% silver, 36.68% carbon, 15.22% oxygen and 5.42% fluorine and (e) Ag/Co/BEM/β-CD contains 36.68% of silver, 32.54% cobalt, 20.22% carbon, 8.42% oxygen and 2.14% fluorine. The FE-SEM pictures and the atom composition of the nano Ag, Ag/Co and BEM are different from those of the Ag/BEM/β-CD and Ag/Co/BEM/β-CD. The alteration of these morphologies is evidence that new nanomaterials have formed.

TEM and EDX images

TEM images of Ag/BEM/β-CD and Ag/Co/BEM/β-CD are displayed in Fig. 5. Nano rod like structures are found in the nanomaterials of the Ag/BEM/β-CD and Ag/Co/BEM/β-CD. Ag nanoparticles were seen in the TEM image to be uniformly spherical particles between 12 and 14 nm in size and Ag/Co nanoparticles were visible between 15 and 17 nm. Ag/BEM/β-CD and Ag/Co/BEM/β-CD nanorod sizes were displayed to be between 100 and 200 nm. The development of inclusion complex nanoparticles is supported by TEM-EDX data: (a) The composition of Ag/BEM/β-CD is 40.16 % silver, 35.15 % carbon, 15.18 % oxygen and 9.51 % fluorine and (b) Ag/Co/BEM/β-CD is 31.84 % silver, 25.31 % cobalt, 21.54 % carbon, 11.26 % oxygen and 10.05 % fluorine. The presence of Ag and Ag/Co along with BEM//β-CD is confirmed by the EDX spectra for the bimetallic nanoparticles. Further, the particle size is measured by TEM: Ag/BEM/β-CD nano – 16.75 nm and Ag/Co/BEM/β-CD nano – 20.31 nm.

ISSN No. 2321-2705 | DOI: 10.51244/IJRSI |Volume XIII Issue III March 2026

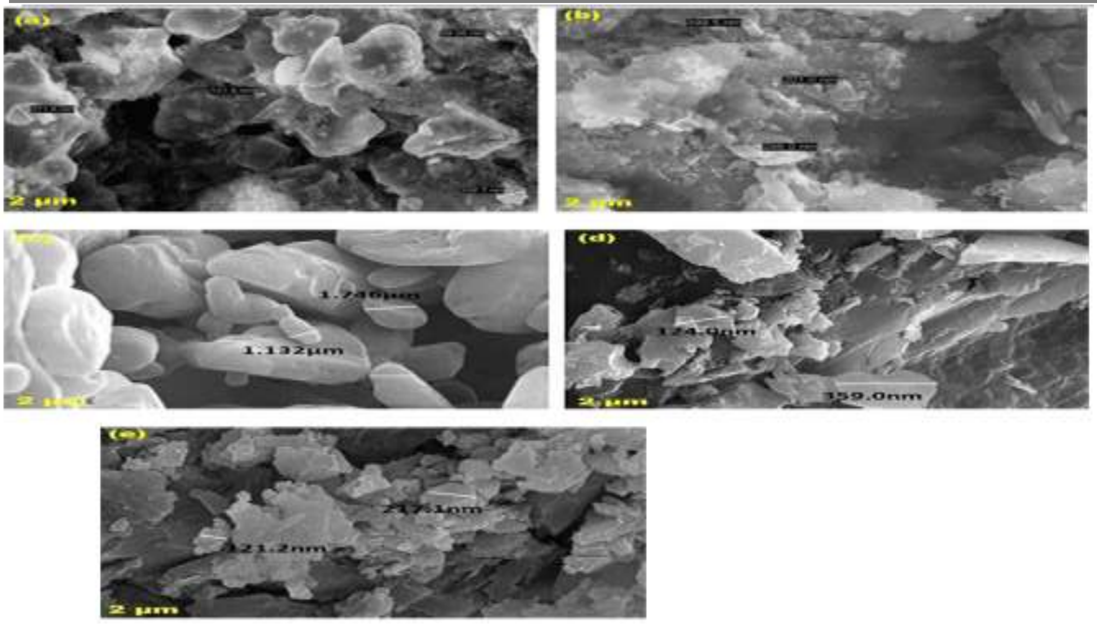

Figure 4. FE-SEM images for (a) Ag nano, (b) Ag/Co, (c) BEM, (d) Ag/BEM/β-CD, (e) Ag/Co/BEM/β-CD

Infrared Spectral Studies

FTIR spectra of Ag, Ag/Co nano, BEM, Ag/BEM/β-CD and Ag/Co/BEM/β-CD were analysed. Due to the conversion of Ag^{+} to Ag^{0} nanoparticles, the FTIR frequencies of the Ag nanoparticles were observed at 3289, 2355, 1633, and 699 cm^{-1}. The frequencies of 3242, 2435, 1641, and 675 cm^{-1} were present in Ag/Co nanoparticles. In Ag/BEM/β-CD and Ag/Co/BEM/β-CD, the above-mentioned frequencies show a considerable modification.

In BEM, the OH group stretching frequency appears at 3320 cm^{-1} was moved to 3250 and 3275 cm^{-1} respectively in Ag/BEM/β-CD and Ag/Co/BEM/β-CD nanomaterials. The C-O frequency of the BEM looks at 1058 cm^{-1} was shifted to 1003 and 1010 cm^{-1} respectively in Ag/BEM/β-CD and Ag/Co/BEM/β-CD nanomaterials. C=O and C=C stretching frequency looks at 1610 cm^{-1} was moved to 1640 and 1632 cm^{-1} respectively in Ag/BEM/β-CD and Ag/Co/BEM/β-CD nanomaterials. C-F stretching frequency seems at 1180 cm^{-1} was moved to 1110 and 1105 cm^{-1} respectively in Ag/BEM/β-CD and Ag/Co/BEM/β-CD nanomaterials.

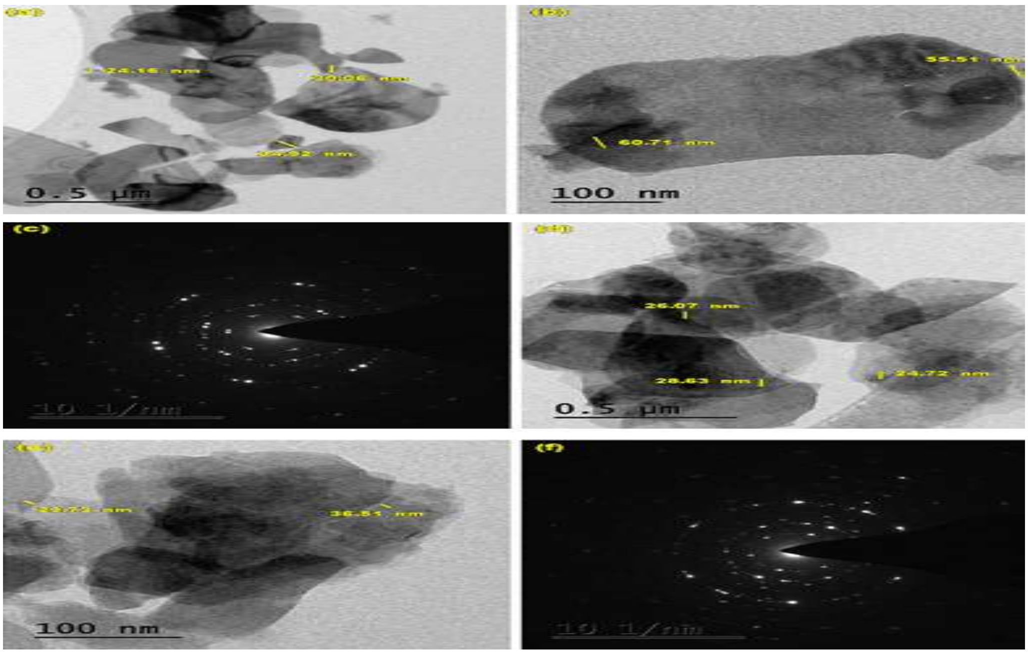

Figure 5. HR-TEM images for (a-c) Ag/BEM/β-CD, (d-f) Ag/Co/BEM/β-CD

ISSN No. 2321-2705 | DOI: 10.51244/IJRSI |Volume XIII Issue III March 2026

The aromatic C-C stretching frequency of the BEM looks at 941 cm^{-1} was shifted to 931 cm^{-1} and 926 cm^{-1} respectively in Ag/BEM/β-CD and Ag/Co/BEM/β-CD nanomaterials. Compared to BEM, the Ag/BEM/β-CD and Ag/Co/BEM/β-CD nanomaterials showed a marked change in the frequencies suggesting that the Ag and Co nanoparticles interact with the BEM and β-CD.

DSC Thermograms

DSC profiles of pure Ag, Ag/Co nano, BEM, Ag/BEM/β-CD and Ag/Co/BEM/β-CD are measured. Ag nano's thermal curve has three exothermic peaks noticed at 198.8, 250.2 and 341.1 °C and three exothermic peaks were visible at 180.4, 205.3 and 290.3 °C in the Ag/Co nanoparticles. BEM drug exhibits three endothermic peaks at 183.5, 254.3, 321.7 °C and three exothermic peaks at 291.2, 330.6, 463.3 °C respectively. In Ag/BEM/β-CD, one endothermic peak appears at 106.4 °C and one exothermic peak at 315.8 °C. In Ag/Co/BEM/β-CD nanomaterial, one endothermic peak was noticed at 116.5 °C, and one exothermic peak at 323.8 °C. The endothermic peaks in the inclusion complex nanomaterials are caused by the loss of water from the CDs. In contrast to the pure BEM, Ag and Ag/Co, a new peak arises in the formation of Ag/BEM/β-CD and Ag/Co/BEM/β-CD inclusion complex nanomaterials.

Powder X-Ray Diffractograms

The XRD method provided additional confirmation of the formation of nanomaterials. The powder form of BEM is given strong sharp peaks in the XRD pattern. With the use of the JCPDS data, the mineral name (3C) and the development of the face-centered cubic (FCC) structure have been confirmed. The JCPDS card number 87-0717 was used to index all of the diffraction peaks with its standard Ag face-centered cube peaks. The values of the hkl plane are found at 111, 200, 220 and 311 respectively. Ag nano powder emerges with four distinct peaks at $2\theta^{o}$ = 38.11°, 44.30°, 64.45° and 77.40° whereas Ag/Co nano shows six peaks at $2\theta^{o}$ = 11.34, 18.15, 22.90, 31.85, 36.05, 64.75.

In Ag/BEM/β-CD nano, there are eleven peaks that can be seen at $2\theta^{o}$ =11.35, 13.29, 17.92, 19.68, 21.60, 33.35, 36.83, 41.19, 47.22, 63.10 and 76.22 and twelve peaks appear in Ag/Co/BEM/β-CD nano at $2\theta^{o}$ =11.38, 13.39, 17.60, 19.61, 21.43, 33.32, 36.61, 39.18, 43.57, 49.23, 63.31 and 76.30. The nanoparticle size is also measured in XRD by the Scherer method: Ag nano - 16.14 nm, Ag/Co – 16.56 nm, Ag/BEM/β-CD nano – 12.65 nm and Ag/Co/BEM/β-CD nano – 16.78 nm. Compared to isolated BEM, the XRD patterns of the Ag/BEM/β-CD and Ag/Co/BEM/β-CD nanomaterials showed a different diffraction pattern and different peak intensities suggesting that inclusion complex nanomaterials were formed. Further, a number of prominent peaks in the 10 to 80-degree range appeared, supporting the formation of metal/BEM/β-CD inclusion complex nanomaterials.

Antibacterial Results

The antibacterial activity of six bacterial pathogens was examined in the samples of BEM, Ag/BEM/β-CD, Ag/Co/BEM/β-CD and drugs (Fig.6). Isolated BEM drug is active for all the bacterial pathogens; the activity is as given below: Escherichia coli -19 mm, Leucobacteralbus-8 mm, Staphylococcus aureus-10 mm, Bacillus pumilis-10 mm, Bacillus subtilis-8 mm and Salmonella typhi-12 mm.

Ag/BEM/β-CD is active in all the pathogens and the activity is as given below: Escherichia coli (15 mm), Leucobacteralbus (10 mm), Staphylococcus aurous (11 mm), Bacillus pumilis (12 nm), Bacillus subtilis (13 mm) and Salmonella typhi (11 mm). Ag/Co/BEM/β-CD is also active in all the above pathogens and the activity is as given below: Escherichia coli (15 mm), Leucobacteralbus (11 mm), Staphylococcus aurous (12 mm), Bacillus pumilis (11 nm), Bacillus subtilis (8 mm) and Salmonella typhi (13 mm). Antibacterial activity results revealed that both Ag/BEM/β-CD and Ag/Co/BEM/β-CD nanomaterials have more antibacterial activity than the isolated BEM drug.

Anticancer Activity of BEM

The anticancer activity of BEM (ID No. 9782) was evaluated using molecular docking methods (Fig. 7). The

ISSN No. 2321-2705 | DOI: 10.51244/IJRSI |Volume XIII Issue III March 2026

2D and 3D docking studies showed interactions between LD and the Epidermal Growth Factor Receptor (EGFR) complexed with epiregulin (EREG) (PDB ID: 5WB7). LD interacted with the 2oh4 protein at Gly1046, Arg1049 &1030 and Asp1050 (conventional hydrogen bond). **The LibDock score was 101.67.**

AutoDock analysis provided the following ADMET results: Solubility level is **3**; Blood-Brain Barrier (BBB) penetration level is **3**; Extended hepatotoxicity (EXT Hepatotoxic MD) is **9.315**; EXT CYP2D6 inhibition prediction is **false**; EXT hepatotoxicity prediction is **false**; EXT Plasma Protein Binding (PPB) prediction is **false**; PPB analysis reflects the unbound fraction (fu) of LD in plasma, which is essential for evaluating its bioavailability. Overall, the results suggest that LD has potential anticancer activity through its interactions with both 1r51 and 2oh4 proteins.

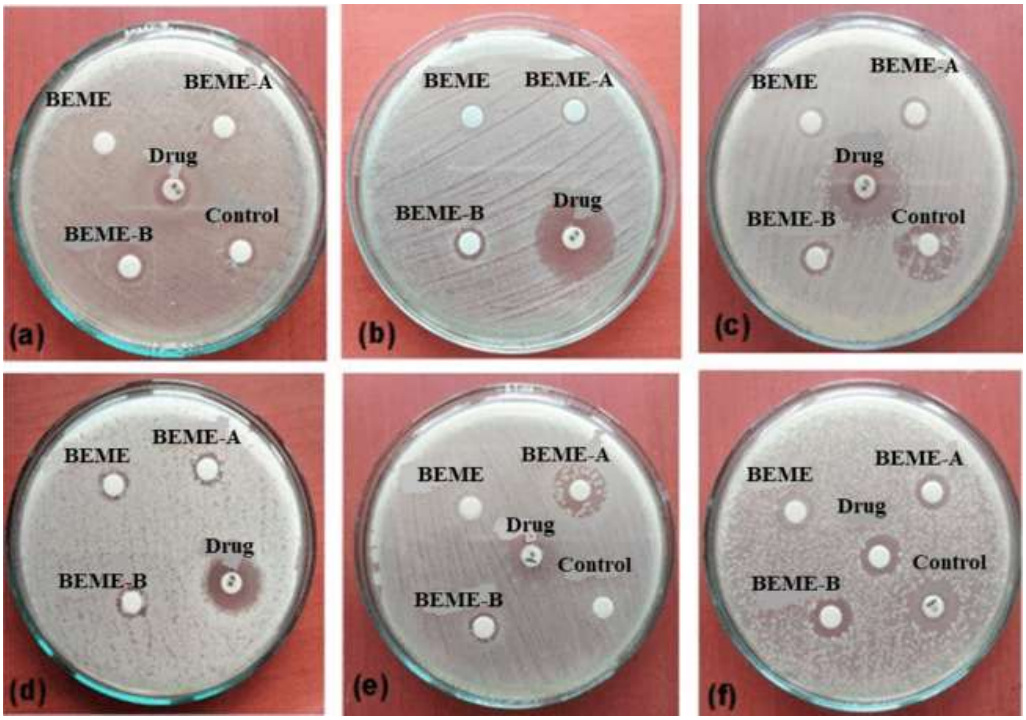

Figure 6. Antibacterial activity images for *(a)* Escherchia coli, (b) Leucobacteralbus, (c) Staphylococcus aureus, (d) Bacillus pumilis, (e) Bacillus subtilis, (f) Salmonella typhi for BEM, Ag/BEM/β-CD, Ag/Co/BEM/β-CD.

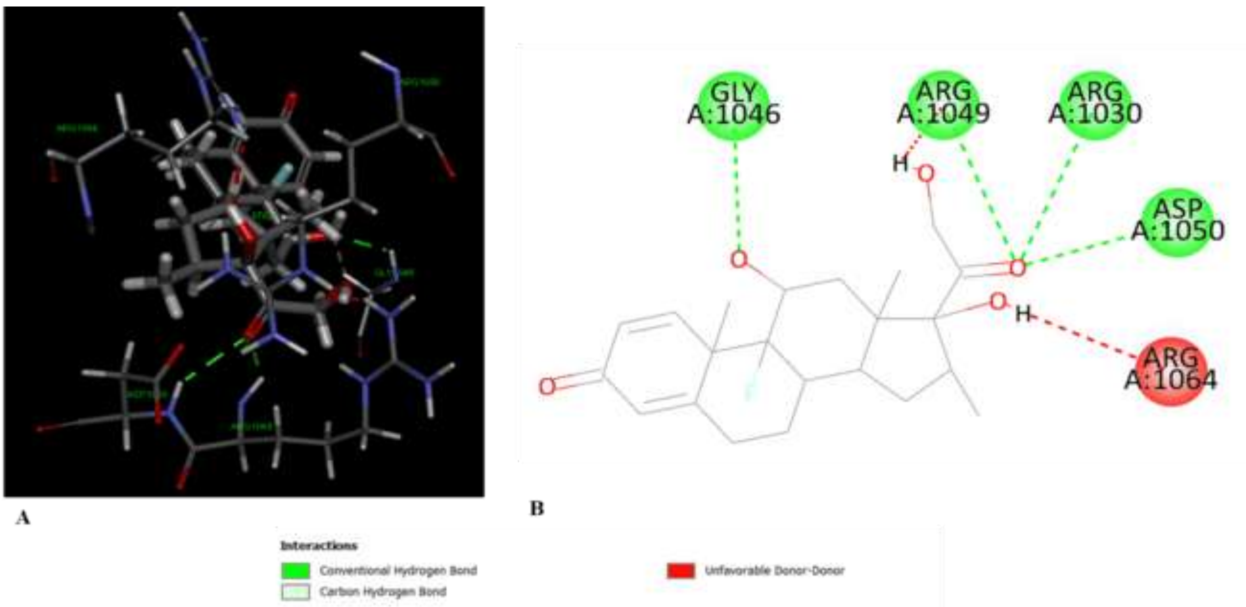

Figure 7. Anticancer activity of BEM with 2oh4 interacting amino acid residues.

CONCLUSION

Different spectral, computational, FE-SEM and TEM techniques were used to analyze Ag/BEM/β-CD and Ag/Co/BEM/β-CD nanomaterials. A Single emission was noticed in the CD and solvents. TEM images showed nanorods are formed in Ag/BEM/β-CD and Ag/Co/BEM/β-CD. Nanoparticle size was measured by TEM-EDS and XRD methods. Antibacterial activity results revealed that the Ag/BEM/β-CD and Ag/Co/BEM/β-CD nanomaterials show more antibacterial activity than isolated BEM drug. Further, BEM exhibits anticancer activity against the 2oh4 protein.

ACKNOWLEDGEMENT

This work was supported by the RUSA PHASE -2.0 [No. 128/A1/ RUSA 2.0, Health and Environment] New Delhi, India. One of the authors, A.Mani is thankful to the RUSA, New Delhi, India for the award of JRF fellowship.

REFERENCES

1. S. Habouti, et al., Synthesis of silver nano-fir-twigs and application to single molecules detection, J. Mater. Chem. **20,** 5215–5219 (2010). https://doi.org/10.1039/B926787H
2. X.H. Hu, C.T. Chan, Photonic crystals with silver nanowires as a near-infrared superlens, Appl. Phys. Lett. **85,** 1520–1522 (2004). https://doi.org/10.1063/1.1786636
3. A.H. Alshehri, et al., Enhanced electrical conductivity of silver nanoparticles for high frequency electronic applications, ACS Appl. Mater. Interfaces **4,** 7007–7010 (2012). https://doi.org/10.1021/am302121z
4. G. Chen, et al., A novel green synthesis approach for polymer nanocomposites decorated with silver nanoparticles and their antibacterial activity, Analyst **139,** 5793–5799 (2014). https://doi.org/10.1039/C4AN01060A
5. A.M. Goodman, et al., The surprising in vivo instability of near-IR-absorbing hollow Au–Ag nanoshells, ACS Nano **8,** 3222–3231 (2014). https://doi.org/10.1021/nn500139f
6. G.B. Braun, et al., Etchable plasmonic nanoparticle probes to image and quantify cellular internalization, Nat. Mater. **13,** 904–911 (2014). https://doi.org/10.1038/nmat3982
7. S.M. Ansari, et al., Cobalt nanoparticles for biomedical applications: Facile synthesis, physiochemical characterization, cytotoxicity behavior and biocompatibility, Appl. Surf. Sci. **414,** 171–187 (2017). https://doi.org/10.1016/j.apsusc.2017.04.037
8. J.K. Lim, et al., Composite magnetic-plasmonic nanoparticles for biomedicine, Nano Today **8,** 98–113 (2013). https://doi.org/10.1016/j.nantod.2013.01.001
9. Q. Zhang, et al., A systematic study of the synthesis of silver nanoplates: is citrate a 'magic' reagent, J. Am. Chem. Soc. **133,** 18931–18939 (2011). https://doi.org/10.1021/ja2080345
10. M.V. Roldán, et al., Electrochemical method for Ag-PEG nanoparticles synthesis, J. Nanopart. Res. **2013,** 524150 (2013). https://doi.org/10.1155/2013/524150
11. G.A. Sotiriou, S.E. Pratsinis, Antibacterial activity of nanosilver ions and particles, Environ. Sci. Technol. **44,** 5649–5654 (2010). https://doi.org/10.1021/es101072s
12. G.A. Sotiriou, et al., Nanosilver on nanostructured silica: antibacterial activity and Ag surface area, Chem. Eng. J. **170,** 547–554 (2011). https://doi.org/10.1016/j.cej.2011.02.025
13. M.M. Kholoud, et al., Synthesis and applications of silver nanoparticles, Arab. J. Chem. **3,** 135–140 (2010). https://doi.org/10.1016/j.arabjc.2010.04.008
14. D. Tien, et al., Discovery of ionic silver in silver nanoparticle suspension fabricated by arc discharge method, J. Alloys Compd. **463,** 408–411 (2008). https://doi.org/10.1016/ j.jallcom.2007.08.083
15. A. Kosmala, et al., Synthesis of silver nanoparticles and fabrication of aqueous Ag inks for inkjet printing, Mater. Chem. Phys. **129,** 1075–1080 (2011). https://doi.org/10.1016/ j.matchemphys.2011.05.065
16. P. Asanithi, et al., Growth of silver nanoparticles by DC magnetron sputtering, J. Nanomater. **2012** (2012) 963609. https://doi.org/10.1155/2012/963609

17. S. Shivaji, et al., Extracellular synthesis of antibacterial silver nanoparticles using psychrophilic bacteria, Process Biochem. **46,** 1800–1807 (2011). https://doi.org/10.1016/j. procbio.2011.06.009
18. G. Li, et al., Fungus-mediated green synthesis of silver nanoparticles using Aspergillus terreus, Int. J. Mol. Sci. **13,** 466–476 (2012). https://doi.org/10.3390/ijms13010466
19. A. Mourato, et al., Biosynthesis of crystalline silver and gold nanoparticles by extremophilic yeasts, Bioinorg. Chem. Appl. **2011,** 546074 (2011). https://doi.org/10.1155/2011/546074
20. L. Ge, et al., Nanosilver particles in medical applications: synthesis, performance, and toxicity, Int. J. Nanomed. **9,** 2399–2407 (2014). https://doi.org/10.2147/IJN.S55015
21. L. Wei, et al., Silver nanoparticles: synthesis, properties, and therapeutic applications, Drug Discov. Today **20,** 595–601 (2015). https://doi.org/10.1016/j.drudis.2014.11.014
22. A. Mani, P. Ramasamy, A.A. Muthu Prabhu, N. Rajendiran, Investigation of Ag and Ag/Co bimetallic nanoparticles with naproxen-cyclodextrin inclusion complex, J. Mol. Struct. **1284,** 135301 (2023). https://doi.org/10.1016/j.molstruc.2023.135301
23. A. Mani, G. Venkatesh, P. Senthilraja, N. Rajendiran, Synthesis and Characterisation of Ag-Co-Venlafaxine-Cyclodextrin Nanorods, Eur. J. Adv. Chem. Res. **5,** 9–16 (2024). https://doi.org/10.24018/ejchem.2024.5.1.147
24. A. Mani, P. Ramasamy, A.A. Muthu Prabhu, P. Senthilraja, N. Rajendiran, Synthesis and Analysis of Ag/Olanzapine/Cyclodextrin and Ag/Co/Olanzapine/Cyclodextrin Inclusion Complex Nanorods, Phys. Chem. Liq. **62,** 196–209 (2024). https://doi.org/10.1080/ 00319104.2023.2297223
25. A. Mani, P. Ramasamy, A.A. Muthu Prabhu, P. Senthilraja, N. Rajendiran, Synthesis and Characterisation of Ag/Co/Chloroquine/Cyclodextrin Inclusion Complex Nanomaterials, J. Sol-Gel Sci. Technol. **115,** 844–856 (2025). https://doi.org/10.1007/s10971-024-06620-5
26. G.M. Morris, D.S. Goodsell, R.S. Halliday, R. Huey, W.E. Hart, R.K. Belew, A.J. Olson, Automated docking using a Lamarckian genetic algorithm and an empirical binding free energy function, J. Comput. Chem. **19,** 1639–1662 (1998). https://doi.org/10.1002/(SICI)1096-987X(19981115)19:14
27. R. Huey, G.M. Morris, A.J. Olson, D.S. Goodsell, Software news and update a semiempirical free energy force field with charge-based desolvation, J. Comput. Chem. **28.** 1145–1152 (2007). https://doi.org/10.1002/jcc.20634
28. T.A. Halgren, Merck molecular force field. I. Basis, form, scope, parameterization, and performance of MMFF94, J. Comput. Chem. **17,** 490–519 (1996). https://doi.org/10.1002/(SICI)1096-987X(199604)17:5/6<490:
29. O. Trott, A.J. Olson, AutoDock Vina: improving the speed and accuracy of docking with a new scoring function, efficient optimization, and multithreading, J. Comput. Chem. **31,** 455–461. (2010) https://doi.org/10.1002/jcc.21334
30. A.D. Hill, P.J. Reilly, Scoring Functions for AutoDock, Methods Mol. Biol. **1273,** 467–474 (2015).
31. T.A. Halgren, Merck molecular force field. VII. Characterization of MMFF94, MMFF94s, and other widely available force fields, J. Comput. Chem. **20,** 730–748 (1999). https://doi.org/10.1002/(SICI)1096-987X(199905)20:7<730::AID-JCC8>3.0.CO;2-T
32. J. Prema Kumari, A.A. Muthu Prabhu, G. Venkatesh, V.K. Subramanian, N. Rajendiran, Effect of solvents and pH on β-cyclodextrin inclusion complexation of 2,4-dihydroxy azobenzene and 4-hydroxy azobenzene, J. Solution Chem. **40,** 327–347 (2011). https://doi.org/10.1007/s10953-010-9639-1
33. T. Stalin, P. Vasantharani, B. Shanthi, A. Sekar, N. Rajendiran, Inclusion complex of 1,2,3-trihydroxybenzene with α- and β-cyclodextrins, Indian J. Chem. A **45A,** 1113–1120 (2006).
34. K. Sivakumar, T. Stalin, N. Rajendiran, Dual fluorescence of diphenyl carbazide and benzanilide: effect of solvents and pH on electronic spectra, Spectrochim. Acta A **62,** 991–999 (2005). https://doi.org/10.1016/j.saa.2005.04.033
35. N. Rajendiran, T. Balasubramanian, Dual fluorescence of syringaldazine, Spectrochim. Acta A **68,** 894–904 (2007). https://doi.org/10.1016/j.saa.2007.01.004
36. A. Antony Muthu Prabhu, R.K. Sankaranarayanan, S. Siva, N. Rajendiran, Intra-molecular proton transfer effects on 2,6-diaminopyridine, J. Fluoresc. **20,** 43–54 (2010). https://doi.org/10.1007/s10895-009-0520-9
37. N. Rajendiran, M. Swaminathan, Spectral characteristics of 4-aminodiphenyl ether in different solvents and various pH, J. Photochem. Photobiol. A: Chem. **93,** 103–108 (1996). https://doi.org/10.1016/1010-6030(95)04189-3

38. G. Venkatesh, R.K. Sankaranarayanan, N. Rajendiran, Azo dye/cyclodextrin: new findings of identical nanorods through 2:2 inclusion complexes, Carbohydr. Polym. **106,** 422–431 (2014). https://doi.org/10.1016/j.carbpol.2014.01.030
39. N. Rajendiran, G. Venkatesh, J. Saravanan, Encapsulation of sulfa pyridine with α- and β-cyclodextrins: spectral and molecular modeling study, J. Mol. Struct. **1054–1055,** 215–222 (2013). https://doi.org/10.1016/j.molstruc.2013.09.035
40. M.J. Jude Jenita, A.A. Muthu Prabhu, N. Rajendiran, Theoretical study of inclusion complexation of tricyclic antidepressant drugs with β-cyclodextrin, Indian J. Chem. A **51A,** 1686–1694 (2012).
41. A.A. Muthu Prabhu, N. Rajendiran, Encapsulation of labetalol and pseudoephedrine in β-cyclodextrin cavity: spectral and molecular modeling studies, J. Fluoresc. **22,** 1461–1474 (2012). https://doi.org/10.1007/s10895-012-1083-8
42. V. G. Venkatesh, A.A. Muthu Prabhu, N. Rajendiran, Azo-hydrazo tautomerism in 1-phenyazo-2-naphthol dyes in various solvents, pH and β-CD, J. Fluoresc. **20,** 961–972 (2010). https://doi.org/10.1007/s10895-010-0642-0
43. G. Venkatesh, R.K. Sankaranarayanan, A.A. Muthu Prabhu, N. Rajendiran, Azonium-ammonium tautomerism and inclusion complexation of 1-(2,4-diaminophenylazo) naphthalene and 4-aminoazobenzene, J. Fluoresc. **21,** 1485–1497 (2011). https://doi.org/10.1007/s10895-011-0835-1
44. J. Venkatesh, R.K. Sankaranarayanan, N. Rajendiran, Cyclodextrin-covered organic micro-rod and micro-sheet derived from supramolecular self-assembly of 2,4-dihydroxy azobenzene and 4-hydroxy azobenzene inclusion complexes, Bull. Chem. Soc. Jpn. **87,** 283–293 (2014). https://doi.org/10.1246/bcsj.20130255
45. J. Prema Kumari, A. Antony Muthu Prabhu, G. Venkatesh, V.K. Subramanian, N.Rajendiran, Effect of solvents and pH on β-CD Inclusion complexation of 2,4-dihydroxy azobenzene and 4-hydroxy azobenzene. J. Solution Chemistry, 40 (2011) 327–347. doi.org/10.1007/s10953-010-9639-1